Time, Frequency & Complexity Analysis for Recognizing Panic States from Physiologic Time-Series

Jonathan Rubin Rui Abreu Shane Ahern Hoda Eldardiry Daniel G. Bobrow
{rubin, rui, heldardi, bobrow}@parc.com, shane@shaneahern.com
Palo Alto Research Center, Inc.
California, United States

ABSTRACT

This paper presents results of analysis performed on a physiologic time-series dataset that was collected from a wearable ECG monitoring system worn by individuals who suffer from panic disorder. Models are constructed and evaluated for distinguishing between pathologic and non-pathologic states, including *panic* (during panic attack), *pre-panic* (preceding panic attack) and *non-panic* (outside panic attack window). The models presented use data fusion to combine both traditional time and frequency domain heart rate variability analysis together with nonlinear/complexity analysis. The best performing model is shown to be a *random forest* classifier that achieves an accuracy of 97.2% and 90.7% for recognizing states of *panic* and *pre-panic*, respectively. The models presented have application in pervasive and ubiquitous mobile and wearable health management systems.

CCS Concepts

•Applied computing → Health informatics; Health care information systems; •Human-centered computing → *Ubiquitous computing;*

Keywords

Physiological data analysis; ECG analysis; Heart rate variability; Feature extraction; Data fusion; Classification

1. INTRODUCTION

Heart rate variability (HRV) measures fluctuations that occur in the intervals between heartbeats. HRV analysis has been shown to have discriminatory power in distinguishing pathologic versus non-pathologic states such as schizophrenia [1], depression [12], stress [16] and heart disease [8, 22]. Traditional HRV analysis relies on computing time-domain statistical parameters to characterize underlying distributions, as well as frequency-domain (Fourier and wavelet-based) power spectral densities for various predefined spectral bands. In additional to traditional time and frequency domains, complexity/nonlinear analysis has emerged as a useful approach for quantifying heart rate dynamics. Complexity analysis captures information about nonlinear dynamical properties and interactions within systems. Unlike traditional time and frequency domain analysis, complexity analysis does not require that the data be stationary or generated by a linear process and it has been shown to reveal "hidden" structural information [8], not necessarily present within traditional HRV analyses.

The main contribution of this work is the presentation and evaluation of a collection of models that rely on data fusion of traditional (time and frequency domain) HRV analysis together with complexity/nonlinear analysis in order to distinguish between pathologic and non-pathologic states associated with panic disorder. We apply time-domain, frequency-domain and complexity analysis to distinguish between states of *panic* (during panic attack), *pre-panic* (one hour before panic attack onset) and *non-panic* (outside panic attack window) in physiologic time-series data. We utilize a physiologic time-series dataset, collected from a population of individuals suffering from panic disorder, where ground truth information was obtained to indicate onset of panic attack symptoms. The dataset was collected from an ambulatory study using a wearable ECG monitoring system [26].

Our analysis compares separately trained time-domain, frequency-domain and complexity-domain models, as well as the fusion of features from all domains to produce combined models. Multiple models are trained using various classifiers and cross validation performed to report classification accuracy. The best performing model is shown to be a random forest classifier, which achieves an accuracy of 97.2% and 90.7% for recognizing states of *panic* and *pre-panic*, respectively.

The predictive models and analysis presented in this work have applications within affective wearable devices and mobile mental health monitoring systems. For example, detection of *panic* states could be utilized within a pervasive wearable system intended for condition management and monitoring. Also, detection of *pre-panic* states (up to one hour before panic attack onset) could be used within an mHealth system capable of delivering timely, useful interventions.

This paper is organized as follows. Section 2 provides background information about ECG, HRV and complexity/nonlinear analysis. Related works are also described that identify pathologic states within physiologic time-series data. Section 3 gives an overview of the data analysis that took place. Section 4 describes, in detail, how features were extracted from the time and frequency domains and com-

PervasiveHealth 2016, May 16-19, Cancun, Mexico

DOI 10.4108/eai.16-5-2016.2263292

plexity analysis. Experimental results and discussion are presented in Section 5, where a comparison of each model constructed is given. Section 6 provides final conclusions.

2. BACKGROUND & RELATED WORK

2.1 Autonomic Nervous System & Heart Rate Variability

The autonomic nervous system is a control system whose functions include control of respiration and cardiac regulation. The autonomic nervous system consists of the sympathetic nervous system (often referred to as the *fight-or-flight* system) and the parasympathetic nervous system (or the *rest-and-digest* system). The sympathetic nervous system has the effect of increasing heart rate, whereas the parasympathetic nervous system slows down heart rate. Competing interactions and influences from both sympathetic and parasympathetic activity leads to variability in heart rate.

Inter-beat (RR) intervals can be measured by determining the interval between neighboring R waves from the QRS complex in an electrocardiogram (ECG), illustrated in Figure 1. This results in a time series consisting of RR intervals.

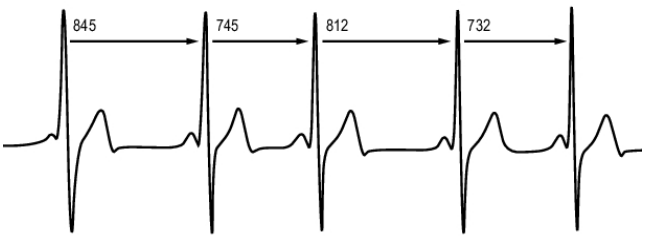

Figure 1: Time intervals (in milliseconds) between R waves in ECG (Source [20]).

HRV analysis captures information about the variability that exists within the RR time series and can provide important insight about the state of health of an individual. Generally speaking, high variability represents healthy behavior, whereas lack of variability often can indicate poor health or disease [8]. Traditional time-domain HRV analysis calculates statistical parameters (e.g. means and variances) from inter-beat (RR) interval time series data. Frequency-domain analysis can indicate whether observed variability reflects *sympathetic* or *parasympathetic* activity. HRV is also governed by complex nonlinear interactions. As such, methods used to analyze nonlinear dynamical systems have been applied to physiology [22] and disease [6]. Computational methods from nonlinear dynamics, fractal analysis and chaos theory have the potential to unveil "hidden" information, not necessarily revealed by traditional forms of statistical and frequency analysis [8, 22].

2.2 Nonlinear/Complexity Background

The basis of nonlinear time-series analysis involves performing a *time-coordinate embedding* [21]. The time-coordinate embedding method attempts to reconstruct the *phase space* of a dynamical system from a sequence of observations of its state. The *phase space* of a dynamical system represents all possible system states. Given a one-dimensional time series of state measurements (such as the interval between heart beats), $x(1), x(2), \ldots, x(N)$, embedding within a higher dimension takes place by constructing delay vectors:

$$x_i = < x(i-(m-1)\tau), \ldots, x(i-\tau), x(i) > \qquad (1)$$

To construct delay vectors, Eq. (1) above requires the selection of two parameters, including the embedding dimension, m, and time lag τ. Delay vectors transform the original one-dimensional time-series measurements into multi-dimensional *reconstructed phase space*. Takens' theorem [27] specifies that for the right selection of m and τ, the embedded dynamics are diffeomorphic (i.e. they have the same topology) to the original state-space dynamics. The result is that reconstruction preserves certain properties of the underlying dynamical system. In particular, *dynamical invariants* are the same across the original underlying dynamical system and the dynamics in reconstruction space given by time-coordinate embedding. Figure 2, illustrates graphically the results of performing time-coordinate embedding from measurements of one state variable of the Lorenz attractor.

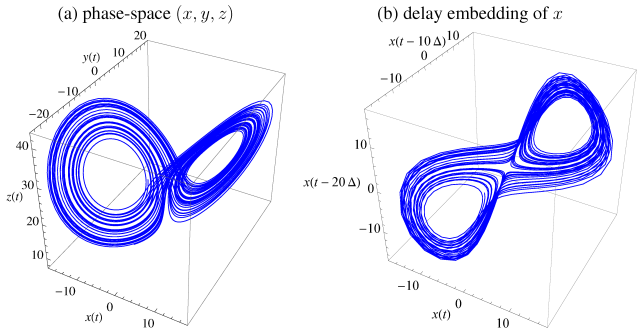

Figure 2: (a) Phase space trajectory of the Lorenz attractor, compared to (b) its reconstruction using time-coordinate embedding (Source [13]).

One caveat, however, is that in order to achieve appropriate reconstruction, the original time series measurements must be a smooth, generic function of at least one state variable and must be uniformly sampled in time. Fortunately, this condition does not typically need to be fully satisfied to achieve satisfactory results in practice.

Performing time-coordinate embedding on inter-beat (RR) interval time-series data allows the computation of *dynamical invariants* that can be used to characterize heart beat dynamics. Section 4.4 (Feature Extraction) details how dynamical invariants, such as the maximal *Lyapunov* exponent, correlation dimension and sample entropy are computed from reconstructed phase space and utilized as features within classifiers for distinguishing between pathologic and non-pathologic states in physiologic time-series data.

2.3 Related Work

Previous works have employed traditional time and frequency domain heart rate variability analysis on physiologic time-series data collected from individuals with panic disorder. [15] collected 24-hour ECG recordings from a population of panic disorder patients and healthy controls. Recordings were analyzed between populations in time and frequency domains. Analysis revealed decreased levels of *sympathetic* nervous system activity, as evidenced by signif-

Measurement	Feature Name	Description
HR	hr	Average heart rate
RR	meanrr	Average RR interval
SDNN	sdnn	Standard deviation of RR intervals, calculated over full time series
SDANN	sdann	Standard deviation of RR interval averages, calculated over windows
SDNNIDX	sdnnidx	Average of RR intervals standard deviations, calculated over windows
pNN50	pnn50	Number of ΔRR larger than 50ms divided by total number of ΔRR
SDSD	sdsd	Standard deviation of ΔRR, calculated over full time series
rMSSD	rmssd	Square root of the average of the squares of ΔRR, calculated over full time series
IRRR	irrr	Difference between first and third quartile of ΔRR, calculated over full time series
MADRR	madrr	Median of ΔRR values, calculated over full time series

Table 1: Time-domain: Statistical features

icantly reduced low frequency power (LF) in panic patients relative to the control group. [23] compared multiple populations with a range of anxiety disorders to healthy controls. Populations included individuals with panic disorder, generalized anxiety, social anxiety and obsessive-compulsive disorder. Baseline comparisons showed that individual with anxiety disorders showed significantly reduced heart rate variability compared to controls. Neither [15] nor [23] included complexity/nonlinear domain measurements within their analysis and both focused on *between-group* comparisons of panic disorder populations and healthy controls.

Instead of *between-group* comparisons, [17, 25] performed *within-group* analysis on a population of panic disorder patients. State changes leading up to panic attack onset (*pre-panic*) were compared with baseline *non-panic* states. Change-point analysis showed that significant changes in physiologic measurements occurred in the time frame leading up to panic attack onset and that the same changes were not witnessed during baseline *non-panic* intervals. Heart rate, HRV, PCO2, tidal volume and breathing rate were included in the analysis performed by [17, 25]. However, a thorough time, frequency and complexity HRV analysis was not performed.

Traditional time and frequency domain HRV analysis, together with complexity/nonlinear analysis has been performed for both *within-group* and *between-group* comparisons for other pathologic states, including depression [12], stress [16], heart disease [8, 22] and schizophrenia [1].

3. ANALYSIS OVERVIEW

The physiologic dataset used within this analysis was collected during an ambulatory study [26] from a population of individuals with panic disorder who experienced regular panic attacks. Subjects wore a wearable 1-lead ECG (250 Hz) monitoring device for up to three weeks. During that time, ground truth information was reported by individuals when panic attacks took place. In total, 19 panic attacks were recorded from 7 study subjects. We refer the reader to [26] for a more comprehensive study description.

First, the inter-beat (RR) time-series data was passed through a simple sliding window artifact filter to remove outliers and ensure acceptable physiological values. RR values that resulted in heart beats per minute of less than 25 or greater than 200 bpm were removed. The dataset was then segmented into three classes including *panic* (beginning when panic attack onset was reported and continuing for ten minutes), *pre-panic* (one-hour before panic attack onset) and *non-panic* (all remaining intervals outside a six hour window surrounding panic attack onset).

Following data segmentation, overlapping sliding windows were run over the data. Feature extraction was performed and feature vectors created. Each sliding window was labeled as *panic*, *pre-panic* or *non-panic*. All sliding windows used 300s intervals and step sizes varied based on the window's class. Sliding window step sizes of 10s, 30s and 300s were used for the *panic*, *pre-panic* and *non-panic* classes, respectively. Variable step sizes were used due to the difference in lengths of data available per class, e.g. ten minutes for *panic* data and one hour for *pre-panic*. Variable step sizes allowed an increase in the amount of data available to train and evaluate models, however, they do not need to be specified to make predictions on new test data instances. In total, 731, 1762 and 1295 *panic*, *pre-panic* and *non-panic* respective windows were used in the analysis.

Within each sliding window, time-domain, frequency-domain and complexity-based features were extracted. A total of 38 features were extracted within each window. Section 4 explains in detail the feature extraction that took place within each domain. Separate models were trained for time-domain only (12 features), frequency-domain only (7 features) and complexity/nonlinear domain only windows (19 features). A combined model that fused all 38 features from each domain was also constructed.

Multiple classifiers were employed for each of the models, including *passive aggressive classifier*, *gradient boosting*, *decision trees*, *ridge classifier*, *support vector machines*, *random forest*, *k-nearest neighbor* and *logistic regression*. Before classification each feature was transformed using a standard (mean normalization) scaler. Default parameters were accepted for each classification algorithm (provided by python's scikit-learn machine learning library). No further parameter tuning was applied. Finally, stratified 10-fold cross validation was used to evaluate each classifier.

The final processed datasets together with the IPython notebooks used to perform the analysis are made publicly available as a github repository at the following location: https://github.com/jrubin01/PervasiveHealth-2016.

4. FEATURE EXTRACTION

4.1 Time-domain: Statistical

(10 features)

Table 1 lists all the statistical parameters derived from a standard time-domain analysis of the RR time series. ΔRR refers to the differences between RR values, i.e. $\Delta RR_i = RR_{i+1} - RR_i$.

4.2 Time-domain: Geometric

(2 features)

Apart from statistical methods, geometric methods can also be used to capture time-domain features. Geometric methods capture information using the probability density distribution of the RR time series. Grouping first occurs by assigning RR intervals into appropriate bins. We selected the standard bin size of 7.8125 ms, which corresponds to $\frac{1}{128}$th of a second. A distribution histogram is created by recording the frequency of RR intervals per bin.

Let D be the distribution histogram, then $D(X)$ reflects the number of RR intervals assigned to bin X. Let $Y = D(X)$, be the maximum of the sample density distribution. Using this information, two geometric measurements are extracted from the distribution histogram:

4.2.1 HRV triangular index

The HRV triangular index is given by the integral of the density distribution divided by the maximum of the density distribution. This is approximated from the distribution histogram by: $\frac{\sum D(X)}{Y}$. Larger values represent lower peaks and increased variability, whereas smaller values would indicate a larger peak and less variability in the sample density distribution.

4.2.2 TINN:

The triangular interpolation of the NN (RR) interval histogram (TINN) is computed by first performing a triangular interpolation over the distribution histogram and maximum sample density, Y, followed by calculating the baseline width of the distribution, i.e $TINN = M - N$, from Figure 3.

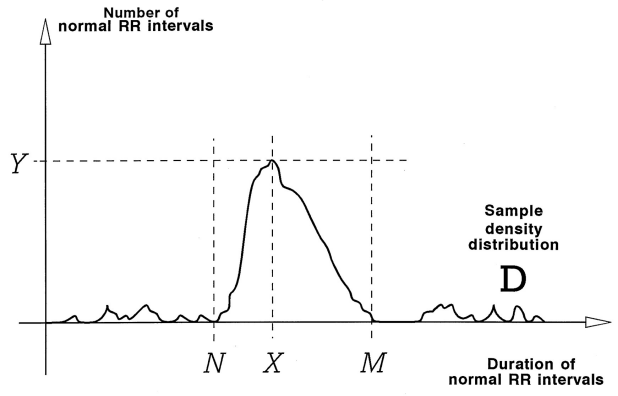

Figure 3: Computation of HRV triangular index and TINN using sample density distribution (Source [19]).

4.3 Frequency-Domain

(7 features)

Frequency-domain analysis is performed using the Fourier transform to extract information about how power distributes as a function of the frequencies found in the inter-beat (RR) time-series. Power spectral density is computed for a range of predefined frequency bands using the Short Time Fourier Transform (STFT) over sliding windows.

Frequency-domain analysis can be used to distinguish between variability in heart rate being attributed to either *sympathetic* or *parasympathetic* activity of the autonomic nervous system. The following frequency bands were used within the spectral analysis and have largely been established within the existing HRV literature [18, 7]:

(ULF) Ultra Low Frequency [0 – 0.003 Hz]

(VLF) Very Low Frequency [0.003 – 0.03 Hz] Thought to be related to the renin-angiotensin system that regulates blood pressure (although this is disputed).

(LF) Low Frequency [0.03 – 0.15 Hz] Believed to largely reflect sympathetic activity, with some parasympathetic activity contributing.

(HF) High Frequency [0.15 – 0.4 Hz] Believed to reflect parasympathetic activity.

Three further frequency-domain parameters are derived from the above values. LFnu and HFnu rescale LF and HF, such that LFnu + HFnu = 100 and LF/HF reflects the normalized power ratio. Large LF/HF ratios (i.e. > 10) can be an indicator of chronic stress.

4.4 Nonlinear domain: Reconstruction space

(5 features)

Recall from Section 2.2 that the purpose of *reconstructed phase space* is to compute *dynamical invariants* to characterize system dynamics. Each of the nonlinear time-series *dynamical invariants* listed below are computed in the following similar manner. First, parameters m and τ are selected to perform a time coordinate embedding. A modified false nearest neighbors method, Cao's algorithm [2], is used to select the embedding dimension, m. The time lag value that results in minimizing mutual information is selected for the parameter τ. Next, ϵ-neighborhoods, $\mathcal{N}_\epsilon(x_i)$ are constructed for a number of delay vectors in reconstruction space. An ϵ-neighborhood consists of all neighboring delay vectors surrounding the vector, x_i, within a specified radius, ϵ. We define the set $\mathcal{N}_\epsilon(x_i)$ as follows:

$$\forall_{j \neq i}, x_j \in \mathcal{N}_\epsilon(x_i), \text{if } \|x_i - x_j\| < \epsilon$$

Choice of the exact distance function used can vary. The total number of items in each ϵ-neighborhood is summed, $C^m(\epsilon)$. Summations are performed for various values of ϵ and the results are plotted on a log-log plot, where the x-axis represents $\log \epsilon$ (where ϵ varies from small to larger values) and the y-axis represents $\log C^m(\epsilon)$. The slope of the linear scaling region in the resulting log-log plot acts as an estimate for the nonlinear-domain parameter in question.

4.4.1 Correlation Dimension

Correlation dimension, $D2$, quantifies the fractal dimensionality of the reconstructed phase space occupied by delay vectors. The Grassberger-Procaccia algorithm [9, 10] is used to estimate correlation dimension, beginning with computation of correlation sums:

$$C^m(\epsilon) = \frac{1}{N(N-1)} \sum_{i=1}^{N} \sum_{j=i+1}^{N} \Theta(\epsilon - \|x_i - x_j\|) \qquad (2)$$

where the Euclidean norm is used to compute the distance between delay vectors, x_i and x_j, in reconstruction space, N

is the total number of delay vectors, ϵ is the specified radius and $\Theta(x)$ is the Heaviside function:

$$\Theta(x) = \begin{cases} 1, & \text{if} \quad x > 0 \\ 0, & \text{if} \quad x \leq 0 \end{cases}$$

Correlation dimension is represented by $D2$ in the relationship: $C^m(\epsilon) \propto \epsilon^{D2}$. Therefore, $D2$ can be estimated as the slope of the linear scaling region in the log-log plot produced by varying radius, ϵ.

4.4.2 *Sample Entropy*

As a single scale value, sample entropy quantifies the degree of predictability or regularity in a time-series [24, 3]. Sample entropy can be computed using the correlation sum from Eq. (2), where Chebyshev distance is used to calculate the distance between delay vectors and radius, ϵ, is chosen to be some proportion of the standard deviation of the time-series.

SampleEn is defined as the natural logarithm of the ratio between the average number of delay vectors within ϵ-neighborhoods for embedding dimension, m, compared to the average number of delay vectors within ϵ-neighborhoods for embedding dimension, $m+1$.

$$SampleEn = \ln\left(\frac{c^m(\epsilon)}{c^{m+1}(\epsilon)}\right) \tag{3}$$

In other words, SampleEn characterizes the proportion of similar time series sequences of length m, compared to the number of similar time series sequences of length $m+1$.

4.4.3 *Maximal Lyapunov Exponent*

The maximal Lyapunov exponent quantifies the strength of chaos within a system by measuring the rate at which trajectories diverge exponentially over time. The maximal Lyapunov exponent is represented by λ in the following relationship:

$$\delta_{\Delta t} \simeq \delta_{t_0} e^{\lambda \Delta t} \tag{4}$$

Here, δ_{t_0} is the distance between two delay vectors at time t_0, and $\delta_{\Delta t}$ is the distance apart in the future after time span, Δt

$$\delta_{t_0} = \|x_i - x_j\|$$
$$\delta_{\Delta t} = \|x_{i+\Delta t} - x_{j+\Delta t}\|$$

Lyapunov exponents describe long-term behavior of a system and are invariant under smooth transformations. They can therefore be estimated from data after performing time coordinate embedding. We use the Kantz algorithm [11], which captures stretching factors over time, to estimate the maximal Lyapunov exponent:

$$S(\Delta t) = \frac{1}{N}\sum_{i=1}^{N} \ln\left(\frac{1}{|\mathcal{N}_\epsilon(x_i)|}\sum_{x_j \in \mathcal{N}_\epsilon(x_i)} |x_{i+\Delta t,-1} - x_{j+\Delta t,-1}|\right) \tag{5}$$

where, x_i, x_j are delay vectors, $\mathcal{N}_\epsilon(x_i)$ is the ϵ-neighborhood surrounding delay vector x_i and the notation $x_{i,-1}$ refers to the last element in vector x_i.

A log-linear plot is composed by computing a variety of stretching factors, $S(\Delta t)$, for various time spans, Δt. Each Δt is plotted against its corresponding $\ln S(\Delta t)$. If a linear scaling region exists in the log-linear plot, its slope can be computed using linear regression and used to estimate the maximal Lyapunov exponent.

4.4.4 *Poincaré Plot*

A Poincaré plot provides a simple method to visualize and quantify variability within a time-series dataset. A 2-dimensional phase space reconstruction is first applied for a given τ and $m = 2$. For an inter-beat interval (RR) time-series choice of $\tau = 1$, the Poincaré plot depicts the correlation between neighboring RR intervals. Fig. 4(a) shows an example. Points on the diagonal identity line represent times when an inter-beat interval, RR_i, was followed by an identical interval, RR_{i+1}, i.e. no variability between neighbors. By fitting an ellipse to the data, two parameters are typically computed:

SD_1 : the standard deviation along the axis perpendicular to the identity line. This value quantifies short-term variability, and

SD_2 : the standard deviation along the identity line. This value quantifies long-term variability over the entire RR series.

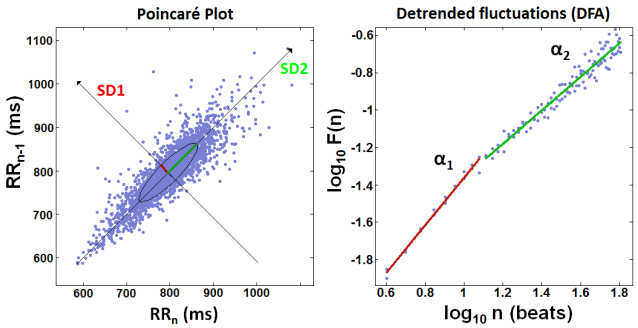

Figure 4: (a) Left: Poincare Plot, (b) Right: Detrended Fluctuation Analysis

4.5 Nonlinear domain: Fractal Analysis

(2 features)

4.5.1 *Detrended Fluctuation Analysis*

Detrended Fluctuation Analysis (DFA) was developed by Peng et al. [22] as a modified root mean square analysis to quantify the amount of self-similarity present in a time series. DFA measures fluctuations over varying time intervals within a time series and compares how fluctuations in small time intervals relate to fluctuations in larger intervals. Typically, two scaling exponents, α_1 and α_2, are computed that capture self-similarity relationships present in data. α_1 describes relationships over short time scales and α_2 describes relationships over longer time scales. An advantage of DFA is that it can be applied to non-stationary time series data, such as physiologic data. Given a sequence of inter-beat (RR) intervals, $RR_1, RR_2, \ldots, RR_N$, first the time series is integrated:

$$y(k) = \sum_{i=1}^{k}(RR_i - \overline{RR}) \tag{6}$$

The integrated time series is then divided into intervals of equal length, n, and a linear regression performed within each segment to determine trend. Detrended fluctuation is

Measurement	Feature Name	Description
Recurrence Rate	rprec	Percentage of recurrence points in a Recurrence Plot
Determinism	rpdet	The percentage of recurrence points which form diagonal lines
Laminarity	rplam	The percentage of recurrence points which form vertical lines
Ratio	rpratio	The ratio between determinism and recurrence rate
Longest diagonal line	rplmax	Length of the longest diagonal line
Longest vertical line	rpvmax	Length of the longest vertical line
Average diagonal line length	rplmean	The average length of the diagonal lines
Adjusted diagonal line length	rplmeanwithoutmain	The average length of the diagonal lines, excluding main diagonal
Divergence	rpdiv	Inverse of longest diagonal line
Trapping time	rpvmean	Average length of the vertical lines.
Entropy	rpentr	Shannon entropy of the probability distribution of diagonal line lengths
Trend	rptrend	The paling of the recurrence plot towards its edges

Table 2: Recurrence quantification analysis feature extraction

calculated as the root mean square difference between the integrated time series, $y(k)$, and its local trend, $y_n(k)$:

$$F(n) = \sqrt{\frac{1}{N}\sum_{k=1}^{N}(y(k) - y_n(k))^2} \quad (7)$$

$F(n)$ is calculated over many time scales, n, and a log-log plot constructed, with $\log_{10}\, n$ plotted on the x-axis and $\log_{10}\, F(n)$ on the y-axis. An example log-log plot is shown in Figure 4(b) with fitted slopes α_1 and α_2. α_1 (short term fluctuations) is the slope obtained from the range $4 \leq n \leq 16$ and α_2 (long term fluctuations) is given by the slope within the range $16 \leq n \leq 64$.

4.6 Nonlinear domain: Recurrence Quantification Analysis

(12 features)

Recurrence refers to the repetition of events within a time series. Recurrence plots [4] can be used to visualize and quantify recurrence by following a trajectory in reconstructed phase space and observing when it returns to the ϵ-neighborhood of points it has visited before. A recurrence matrix is computed as follows:

$$M_{ij} = \Theta\left(\epsilon - \|x_i - x_j\|\right) \quad (8)$$

where x_i and x_j are delay vectors and ϵ determines the size of the neighborhood. $M_{ij} = 1$, if the trajectory within reconstructed phase space returns at time j to the same ϵ-neighborhood it was in at time i, otherwise $M_{ij} = 0$. The recurrence matrix can be visualized by plotting black points where $M_{ij} = 1$ and white points where $M_{ij} = 0$.

Recurrence can be quantitatively characterized by extracting various statistical parameters from a recurrence plot matrix. Table 2 lists each parameter that was extracted from recurrence plots and utilized within a feature vector for performing eventual classification. Table 2 has been adapted from [14] and [5], which is the software package we used to perform recurrence quantification analysis.

5. RESULTS

Table 3 presents accuracy results for the trained *panic* prediction models based on stratified 10-fold cross validation. The results shown are from globally trained models (i.e. not subject specific) performing binary classification of panic vs. non-panic instances. Comparisons are provided for the time, frequency and nonlinear domains, as well as the combined domain model. In total, eight classifiers are evaluated, as well as a baseline classifier that simply always predicts the most frequently occurring class. In all cases, the *random forrest* classifier is the best performing (highlighted in bold). Further, for all classifiers, use of the combined model that fuses features together from all domains, results in at least some level of performance improvement. The top performing combined model *random forrest* classifier achieves an accuracy of 97.2%.

Table 4 provides equivalent accuracy results for the *pre-panic* prediction models. Results shown are from globally trained models performing binary classification of pre-panic vs. non-panic instances. Once again, the *random forrest* classifier achieves the greatest accuracies, except in the case of the frequency-domain only, where the *gradient boosting* classifier performs best. The combination of domains again achieves the best accuracy for all classifiers and the top performing *random forrest* classifier achieves an accuracy of 90.7%.

Next, we investigated feature importance from the top performing *random forrest* classifiers. Fig. 5 shows the relative importance of all 38 features for both *panic* (left) and *pre-panic* (right) prediction models. In both cases, Shannon entropy calculated from recurrence quantification is identified as the most discriminatory feature. Mean and median inter-beat RR values from the time-domain are also rated highly, as well as average heart rate for the *panic* prediction model.

5.1 Discussion

The results of our analysis show that by combining time, frequency and nonlinear domain parameters, >90% accuracy can be achieved when distinguishing between *panic*, *pre-panic* and *non-panic* states in physiologic time-series data. Greater accuracy is achieved recognizing *panic* states compared to *pre-panic*. It makes sense that physiological measurements recorded during a panic attack would differ more markedly from non-panic data, compared with measurements leading up to panic attack onset. Our results further show that separate time, frequency and nonlinear domains produce models which vary in classification accuracy. The frequency-only domain produces models with the lowest accuracy. Tables 3 and 4 show that both time and nonlinear domains outperform frequency-domain models for all classifiers. For *panic* prediction models, the nonlinear-domain

Model	Time-domain only	Frequency-domain only	Nonlinear-domain only	Combined
Passive Aggressive	0.620	0.564	0.691	0.727
Gradient Boosting	0.887	0.744	0.931	0.958
Decision Tree	0.905	0.782	0.913	0.931
Ridge Classifier	0.741	0.692	0.737	0.818
Support Vector Machine	0.814	0.698	0.877	0.922
Random Forest	**0.948**	**0.795**	**0.950**	**0.972**
k-Nearest Neighbor	0.894	0.741	0.899	0.948
Logistic Regression	0.740	0.697	0.753	0.825
Baseline	0.639	0.639	0.639	0.639

Table 3: Global model: panic vs. non-panic accuracy scores

Model	Time-domain only	Frequency-domain only	Nonlinear-domain only	Combined
Passive Aggressive	0.604	0.565	0.684	0.714
Gradient Boosting	0.802	**0.700**	0.857	0.887
Decision Tree	0.788	0.668	0.834	0.873
Ridge Classifier	0.705	0.647	0.787	0.806
Support Vector Machine	0.756	0.658	0.837	0.865
Random Forest	**0.820**	0.688	**0.871**	**0.907**
k-Nearest Neighbor	0.809	0.683	0.851	0.874
Logistic Regression	0.707	0.654	0.796	0.813
Baseline	0.576	0.576	0.576	0.576

Table 4: Global model: pre-panic vs. non-panic accuracy scores

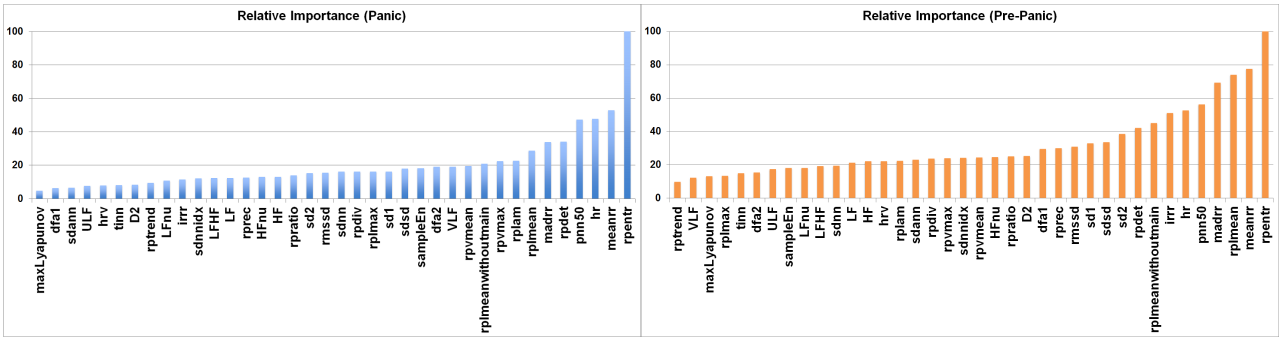

Figure 5: (a) Panic prediction model feature importance, (b) Pre-panic prediction model feature importance

results in greater accuracies over the time-domain for all but one classifier (*ridge* classifier) and for *pre-panic* prediction models, nonlinear-domain features always improve accuracy over time-domain features. The improved accuracy of nonlinear-domain models over time and frequency domains is likely due to the fact that complexity analysis is better able to handle non-linearity, as well as non-stationarity introduced into the data due to movement and activity.

There are a number of limitations in the present analysis. First, complexity analysis that relies on reconstructed state space typically requires that the identification of linear scaling regions in log-log plots be performed with a human-in-the-loop. For example, parameters such as correlation dimension and maximal Lyapunov exponent require the specification of an x-axis range where regression will be performed. In the current complexity/nonlinear analysis no attempt has been made to locate linear scaling regions. Instead, regression is performed over the entire x-axis range. Future analysis would benefit by introducing either automatic or human-in-the-loop linear scaling region identification. Second, it is possible that the size of the sliding windows used may be too small to entirely reflect the inter-beat (RR) interval behavior. In particular, parameters such as SDANN and ULF are two standard HRV measures where it is known that accuracy is limited given short window sizes [18]. These two limitations imply time and frequency parameters produced during feature extraction, as well as the dynamical invariants computed from complexity analysis may not necessarily approximate characteristics of underlying system dynamics. Nevertheless, while the above limitations should be taken into account, the objective of the current work is not to precisely characterize heart beat dynamics, but instead to utilize the computed parameter values to accurately differentiate between pathologic and non-pathologic states.

6. CONCLUSIONS

We have shown that *panic*, *pre-panic* and *non-panic* states can be recognized with reasonable accuracy within physiologic time-series data. Separate models were compared based on feature extraction in time, frequency and nonlin-

ear/complexity domains. Models that combined domains via data fusion achieved the greatest accuracy. While further modifications and improvements are required, our analysis demonstrates the potential for these models to be utilized within affective wearable health monitoring applications. Further, the approach presented and feature extraction methods used are applicable for classifying other types of pathologic states from physiologic time-series data, including emotional stress, depression and heart disease.

7. REFERENCES

[1] S. Boettger, D. Hoyer, K. Falkenhahn, M. Kaatz, V. K. Yeragani, and K.-J. Bär. Altered diurnal autonomic variation and reduced vagal information flow in acute schizophrenia. *Clinical Neurophysiology*, 117(12):2715–2722, 2006.

[2] L. Cao. Practical method for determining the minimum embedding dimension of a scalar time series. *Physica D: Nonlinear Phenomena*, 110(1):43–50, 1997.

[3] M. Costa, A. L. Goldberger, and C.-K. Peng. Multiscale entropy analysis of complex physiologic time series. *Physical review letters*, 89(6):068102, 2002.

[4] J.-P. Eckmann, S. O. Kamphorst, and D. Ruelle. Recurrence plots of dynamical systems. *Europhys. Lett*, 4(9):973–977, 1987.

[5] C. A. Garcıa, A. Otero, and X. Vila. Getting started with RHRV, 2013.

[6] L. Glass and J. Milton. *Dynamical Disease: Mathematical Analysis of Human Illness*. American Institute of Physics, 4 1995.

[7] A. L. Goldberger, L. A. Amaral, L. Glass, J. M. Hausdorff, P. C. Ivanov, R. G. Mark, J. E. Mietus, G. B. Moody, C.-K. Peng, and H. E. Stanley. PhysioBank, PhysioToolkit, and PhysioNet components of a new research resource for complex physiologic signals. *Circulation*, 101(23):e215–e220, 2000.

[8] A. L. Goldberger, L. A. Amaral, J. M. Hausdorff, P. C. Ivanov, C.-K. Peng, and H. E. Stanley. Fractal dynamics in physiology: alterations with disease and aging. *Proceedings of the National Academy of Sciences*, 99(Suppl 1):2466–2472, 2002.

[9] P. Grassberger and I. Procaccia. Characterization of strange attractors. *Physical review letters*, 50(5):346, 1983.

[10] P. Grassberger and I. Procaccia. Measuring the strangeness of strange attractors. *Physica D*, pages 170–189, 1983.

[11] H. Kantz and T. Schreiber. *Nonlinear Time Series Analysis*. Cambridge University Press, 2 edition, 1 2004.

[12] S. J. Leistedt, P. Linkowski, J. P. Lanquart, J. Mietus, R. B. Davis, A. L. Goldberger, and M. D. Costa. Decreased neuroautonomic complexity in men during an acute major depressive episode: analysis of heart rate dynamics. *Translational psychiatry*, 1(7):e27, 2011.

[13] G. Martius and E. Olbrich. Quantifying emergent behavior of autonomous robots. *Entropy*, 17(10):7266–7297, 2015.

[14] N. Marwan, M. C. Romano, M. Thiel, and J. Kurths. Recurrence plots for the analysis of complex systems. *Physics Reports*, 438(5):237–329, 2007.

[15] R. McCraty, M. Atkinson, D. Tomasino, and W. P. Stuppy. Analysis of twenty-four hour heart rate variability in patients with panic disorder. *Biological psychology*, 56(2):131–150, 2001.

[16] P. Melillo, M. Bracale, L. Pecchia, et al. Nonlinear heart rate variability features for real-life stress detection. case study: students under stress due to university examination. *Biomed Eng Online*, 10(1):96, 2011.

[17] A. E. Meuret, D. Rosenfield, F. H. Wilhelm, E. Zhou, A. Conrad, T. Ritz, and W. T. Roth. Do unexpected panic attacks occur spontaneously? *Biological psychiatry*, 70(10):985–991, 2011.

[18] J. E. Mietus and A. L. Goldberger. Basic time and frequency domain measures. https://physionet.org/tutorials/hrv-toolkit. Accessed: 2016-01-15.

[19] T. F. of the European Society of Cardiology the North American Society of Pacing Electrophysiology. Heart rate variability standards of measurement, physiological interpretation, and clinical use. *Circulation*, 93:1043–1065, 1996.

[20] R. J. Oweis and B. O. Al-Tabbaa. QRS detection and heart rate variability analysis: A survey. *Biomedical Science and Engineering*, 2(1):13–34, 2014.

[21] N. H. Packard, J. P. Crutchfield, J. D. Farmer, and R. S. Shaw. Geometry from a time series. *Physical review letters*, 45(9):712, 1980.

[22] C.-K. Peng, S. Havlin, H. E. Stanley, and A. L. Goldberger. Quantification of scaling exponents and crossover phenomena in nonstationary heartbeat time series. *Chaos: An Interdisciplinary Journal of Nonlinear Science*, 5(1):82–87, 1995.

[23] A. Pittig, J. J. Arch, C. W. Lam, and M. G. Craske. Heart rate and heart rate variability in panic, social anxiety, obsessive–compulsive, and generalized anxiety disorders at baseline and in response to relaxation and hyperventilation. *International Journal of Psychophysiology*, 87(1):19–27, 2013.

[24] J. S. Richman and J. R. Moorman. Physiological time-series analysis using approximate entropy and sample entropy. *American Journal of Physiology - Heart and Circulatory Physiology*, 278(6):H2039–H2049, 2000.

[25] D. Rosenfield, E. Zhou, F. H. Wilhelm, A. Conrad, W. T. Roth, and A. E. Meuret. Change point analysis for longitudinal physiological data: detection of cardio-respiratory changes preceding panic attacks. *Biological psychology*, 84(1):112–120, 2010.

[26] J. Rubin, H. Eldardiry, R. Abreu, S. Ahern, H. Du, A. Pattekar, and D. G. Bobrow. Towards a mobile and wearable system for predicting panic attacks. In *Proceedings of the 2015 ACM International Joint Conference on Pervasive and Ubiquitous Computing*, pages 529–533. ACM, 2015.

[27] F. Takens. *Detecting strange attractors in turbulence*. Springer, 1981.